Theoretical investigation of doped $LiMg_{1-x}Y_xN$ (Y = Ag, Cu, Mn, Zn) for RRAM application

S. Kiran[a], U. Rasheed[b], M. Imran[c*], F. Hussain[b] , N. A. Niaz[b], E. A. Khera[d], R. M. A. Khalil[b], A. Nazir[a]
[a]*Institute of Physics,The Islamia University of Bahawalpur, Pakistan*
[b]*Materials Simulation Research Laboratory (MSRL), Department of Physics, Bahauddin Zakariya University Multan Pakistan, 60800*
[c]*Department of Physics, Govt. College University Faisalabad, 38000, Pakistan*
[d]*Department of Physics Bahawalnagar Campus, The Islamia University of Bahawalpur, 63100 Pakistan*

With the assistance of a First Principles research based on density functional theory, electronic and optical characteristics of the $LiMg_{1-x}Y_xN$ (Y = Ag, Cu, Mn, Zn) are examined. The influence of magnetic (Mn, Zn) and non-magnetic (Ag, Cu) dopants without and with nitrogen vacancies (V_N) on the electronic and optical characteristics of optimized LiMgN is investigated by determining the contribution of each atom towards charge redistribution. The isosurface charge density and integrated charge density plots depicted the development of conduction filaments. Electronic properties showed best conductivity that makes the studied composites vibrantly useful for resistive switching memory applications. The optical analysis showed that considered composite possess conductivity and absorptivity in a wide range of incident photon energies with their nominal reflectivity. The least formation energy and greatest conductivity observed in LiMgN-Mn-V_N proved it to be the most stable. Entire analyses portray that considered compounds are potential candidates for applications in optoelectronic devices.

(Received January 17, 2022; Accepted May 2, 2022)

Keywords: DFT, Resistive switching, Electronic conductivity, PBE-GGA, Conduction filaments

1. Introduction

Data storage has exploded in response to the emergence of the information age and the rapid advancement of the internet, and traditional storage techniques are unable to keep up requirements [1]. In Non-volatile memory (NVM) devices, flash memory is now the most common product. Continuous growth, on the other hand, will eventually bring it to its physical limits, resulting in retention degradation and serious reliability concerns. As a result, several new technologies are expected to replace flash memory in near future [2]. Optoelectronic memristors have a lot of potential as a next-generation storage device since they use a combination of optical and electrical ways to monitor the resistive switching (RS). The possible application of the resistive switching (RS) effect in the next generation non-volatile memory, disclosed as resistive random-access memory (RRAM), prompted a surge in study a few years ago [1]. The most recent advancement in RRAM has brought the production of highly competent gadgets to the forefront. The metal-insulator-metal (MIM) structure is the most common memristor configuration [2]. The structure compromises as insulating layer is sandwich among two metal electrodes. The metals used as electrodes might be active (Ag, Ni, and Cu) or inert (Au, Pt and Pd). The resistive switching (RS) material sandwiched between these two electrodes is usually transition metal oxides (TMOs) and rare earth oxides [3]. The basic principle of RRAM work on high resistance state(HRS) and low resistance state(LRS)[4]. Due to lot of advantages to use semiconductor to improve conductivity of RRAM many investigations are done on this [5].The Nowatny Juza

*Corresponding authors: imraniub86@gcuf.edu.pk
https://doi.org/10.15251/JOR.2022.183.301

phases A^{I} B^{II} C^{V} by means of A^{I} = Li, Ag, Cu; B^{II} = Be, Mg, Cd, Zn and C^{V}= N, P, Sb, As, Bi stand acknowledged extensive band gap semiconductors [6, 7]. A^{I} B^{III} C^{IV} for example LiAlSi [8] and LiGaSi [9] and A^{II} B^{II} C^{IV} phases e.g. Mg_2Si [10] as well fit in this group are also a semiconductor. Band gaps for these composite LiZnN, LiMgP and LiMgN are reported earlier [6, 11 and 12]. The crystal structure and band gaps of LiMgX compounds have been the topic of several investigations [13–17]. N.Safikah *et. al.* calculated the electronic and optical properties of LiMgN half heusler (HH) alloy [5]. Kalarasse *et. al.* have looked at the linear optical characteristics [18] of LiMgX. Bacewicz*et. al.* and Kuriyama *et. al.* produced a variety of semiconductors, including LiZnP, LiCdP, LiZnAs, LiZnN, LiMgP, LiMgAs and LiMgN evaluated their lattice characteristics and band gap nature in theoretical investigations [14]. Recently our group studied electro-optical of XYZ (X = Li; Na and K, Y = Mg, Z = N; P; As; Sb and Bi) inside full-potential linearized augmented plane wave [19].Many studies show that dopants (metal ions) with and without oxygen vacancies improve the performance of non-volatile RRAM systems [20].Doping is thought to be a good technique to improve RRAM performance [21].

In this study electronic and optical property of cubic LiMgN is investigated. This study is aimed to investigate the impact of substitutional dopants (Ag, Cu, Mn, Zn) in place Mg and dopants and nitrogen vacancies (V_N) on LiMgN. Electronic and optical characteristics are examined in order to calculate the suitability of the studied composites for designing efficient RRAM devices. The investigated LiMgN are expected to have interesting uses in photo responsive memristors and related devices.

2. Computational methodology

Super cell of cubic LiMgN represent in Figure 1(a) is made then dopants was doped in place of one atom of Mg, coupled with a single nitrogen vacancy, after confirmation of LiMgN charge filament generation behavior. The formation energies, isosurface charge density, electronic density of states (DOS), partial electronic density of states (PDOS) and integrated charge density were performed using generalized gradient approximation (GGA) along with Perdew, Burke and Ernzerhof (PBE) functional with the help of Vienna *ab initio* simulation package (VASP) [22-25], based on density functional theory. Hubbard parameter values of 2.0 eVand 2.5 eV were used for Ag and Cu respectively. For computations, the valence electron configurations ofLi $2s^1$,Mg$3s^2$, N$2s^2 2p^3$, Ag$4d^{10}5s^1$,Cu $3d^{10}4s^1$, Mn$3d^5 4s^2$, Zn$3d^{10}4s^2$were used. Plane-waves with cut-off energy of 410 eV were used to guide the convergence tests for total energy of the system with regard to electron wave functions. The ionic positions, cell volume and lattice parameters of the system were fully relaxed with conjugate gradient (CG) method until Hellmann Feynman forces became smaller than 0.02 eV/Å. While, the energy convergence criteria were met possibly at 1×10^{-5} eV [24, 25]. The most popular scheme for these calculations was Monkhorst Pack (MP) [26, 27] which was applied for k-point sampling. The MP grid was chosen to be 8×8×8 for whole calculations. Moreover, stability approximation of optimized structures is assessed by overall formation energy (ΔE) of undoped and doped systems as given in Figure 1(b).The ΔE of the doped $LiMg_{1-x}Y_xN$ (Y=Ag, Cu, Mn and Zn) and $LiMg_{1-x}Y_xN$-V_N (Y=Ag, Cu, Mn and Zn) lattice are calculated by means of subsequent equation [28, 29].

$$\Delta E = E_{tot}(doped\ composie) - E_{tot}(undoped\ composite) - E_{tot}(dopant) \quad (1)$$

In formation energy calculations negative sign is signifying that studied composites are energetically stable and can be organized experimentally with ease [30, 31]. The calculated results show that the whole formation energy for LiMgN-Mn-V_N is comparatively smaller than all other studied composites. This reveals that the LiMgN-Mn-V_N system is comparatively more stable.

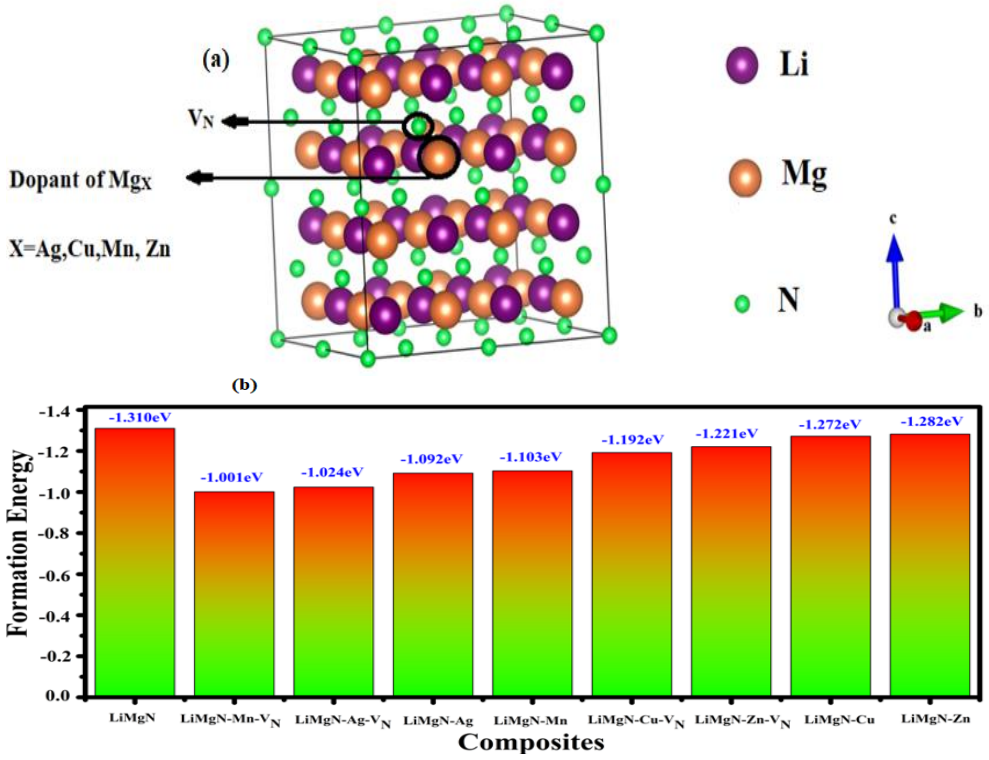

Fig. 1. (a) Represent pure LiMgN, here purple color represents Li atom, orange color represents Mg atoms and green color represents N atoms and (b) Represent Formation energy of all composites.

3. Electronic properties

The distribution of the electrons is inspected with help of calculations of isosurface charge density, integrated charge density and density of states (DOS). DOS verses energy plots shown in Figure 2, here blue dashed line shows the Fermi level (E_F) which is lying at 0 eV. The right side of E_F is conduction band (CB) and left side of E_F shows Valance band (VB). DOS plots of all composite shown in Figure 2, using GGA+PBE approach are analyzed. In case of pure LiMgN (Figure 2(a)) observed band gap is 2.4 eV. Same band gap of LiMgN was reported earlier by N. Safikah*et.al*.[5]. In case of all doped composites the CB minima is shifted towards low energy region of CB but this shift is maximum in case of LiMgN-Mn. In case of dopant $+V_N$CB minima is also shifted towards low energy region of CB as well as defect states also appear near the Fermi level due to vacancy of nitrogen atom. But this shift is maximum in case of LiMgN-Mn-V_N composite (Figure 2(f)).It is observed that dopant without and with V_N decreases the band gap. But this reduction in band gap is comparatively larger in case of LiMgN-Mn-V_N (Figure 2(f)).Hence conductivity of whole system is increased by Mn doping and Mn doping with V_N leading to resistance transition from insulating to conducting behavior and take great part in directly generating conduction filament. Presence of localized states in the occupied/unoccupied part VB/CB is a manifestation of good electronic mobility. This makes our doped systems essential in the field of electronic devices.

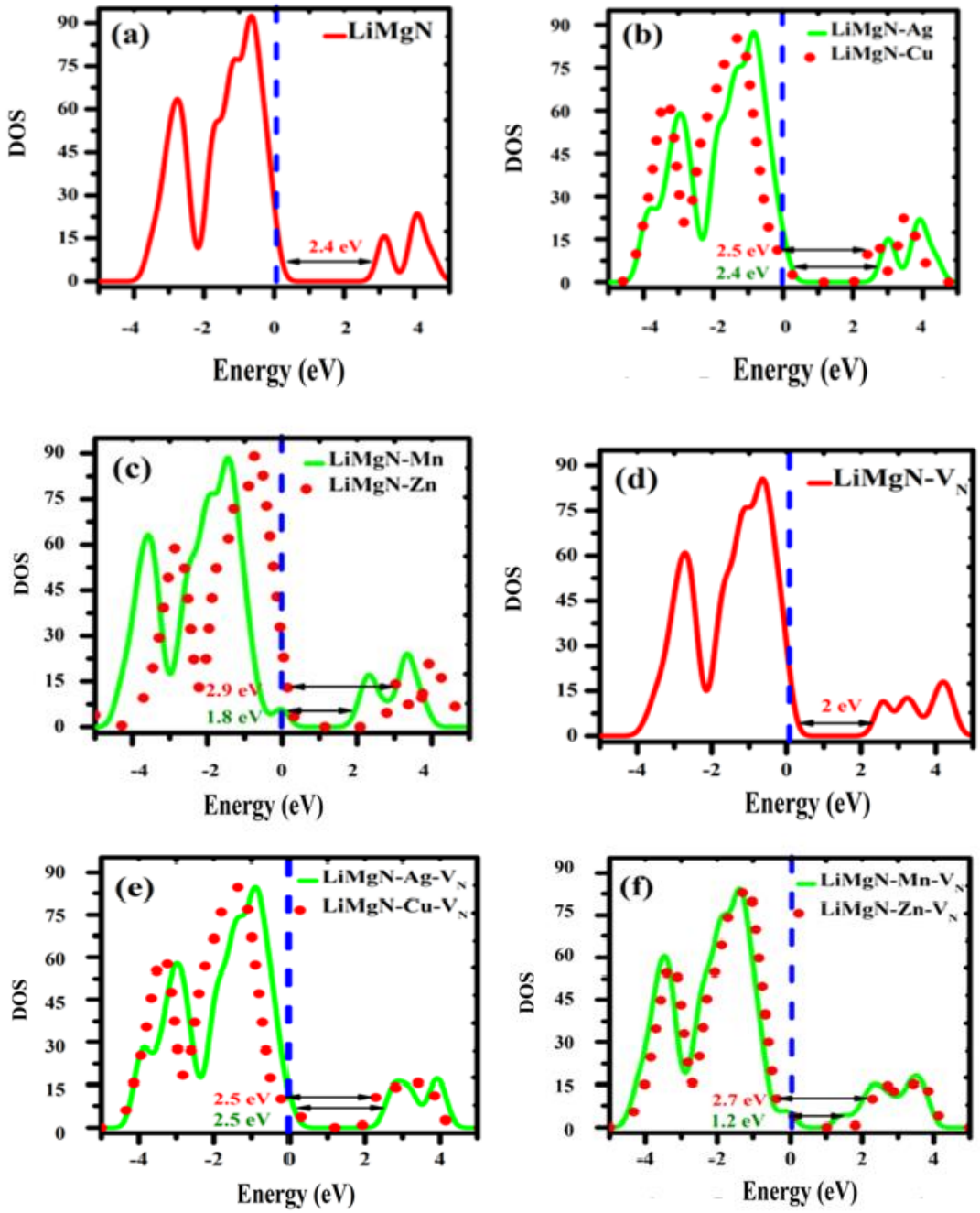

Fig. 2. DOS of (a-c) composite $LiMg_{1-x}Y_xN$ (Y= Ag, Cu, Mn, and Zn) and (d-f) $LiMg_{1-x}Y_xN$-V_N (Y= Ag, Cu, Mn, and Zn). Dashed line (blue) representing Fermi level (E_F) with left and right side of E_F representing VB and CB region respectively.

4. Charge density

Isosurface charge density difference for $LiMg_{1-x}Y_xN$ (Y = Ag, Cu, Mn, Zn) is calculated as:

$$\nabla\rho = \rho_{doped\ composite} - (\rho_{undoped\ composite} + \rho_{dopant}) \quad (2)$$

Here $\nabla\rho$, $\rho_{doped\ composite}$, $\rho_{undoped\ composite}$ and ρ_{dopant} is charge density difference, charge density of doped and undoped respectively. Figure 3, 4 and 5 show the isosurface plots of the doped and doped+V_N LiMgN. Purple, orange and green colored atoms represent Li, Mg and N

atoms respectively. Integrated planar charge density along z-axis normal to (x, y) plane has also been computed for confirmation of charge redistribution for a more thorough understanding of dopant function with different charge states. With the aid of this equation, we evaluated the periodic geometry of a super cell in the (x, y) plane and averaged the density over the (x, y) plane [32].

$$\rho(z) = \int \rho(r)dxdy \tag{3}$$

Integrated charge density as a function of distance in the z direction is given in Figures 3, 4 and 5. Charge accumulation and depletion are represented by up and down humps, respectively. In integrated planer charge density plot the positive shift of charge density exposed charge accumulation with charge depletion (negative shift). Bhaskar Chilukuri *et. al.* used identical sort of description aimed at their planar charge density as well as iso-surface charge density results [33].In Figure 3(a), positive value of integrated charge density is representing charge accumulation in case of LiMgN-V_N. This charge accumulation is also confirmed by Isosurface charge density representing accumulation of charge around V_N(Figure 3(b)).This behavior is also observed from defect states in band gap region of DOS calculation in Figure 2 (d).

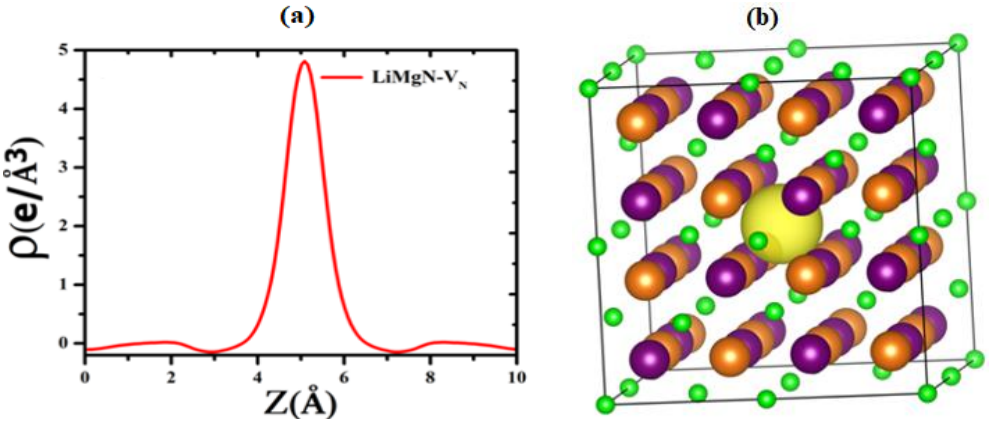

Fig. 3. (a) Integrated planer charged density and (b) Isosurface charge density plots of composite LiMgN-V_N. Where purple, orange and green balls represent Li, Mg and N atoms, while yellow color represent charge accumulation.

Figure 4(a) represents isosurface charge density of LiMgN-Ag. Depletion of charge around dopant is observed in this case which is also confirmed from integrated planner charge density (green line) in Figure 4(b).Red line in Figure 4(b) shows that comparatively larger amount of charge is depleted by Cu atom in case of LiMgN-Cu. This depletion of charge around dopant is also confirmed from isosurface charge density given in Figure 4(c).Non-magnetically doped LiMgN with vacancy of nitrogen atom gives different behavior due to presence of nitrogen vacancy. Figure 4(d) represent isosurface charge density having depletion Ag dopant and small amount of accumulation also observed around V_N. This behavior is also confirmed from Figure 4(e), green line represents integrated planner charge density of LiMgN-Ag-V_N. Red line for LiMgN-Cu-V_N shows comparatively larger amount of depletion around dopant. This behavior is also confirmed from Figure 4(f).In Figure 2 DOS calculation also satisfied this behavior of Figure 4.As a result of this charge redistribution in both cases, dopant and V_N support more conduction process which is beneficial for development of conductive filaments (conductive route) that is required for RS events. By collecting and depleting additional charges, dopant along with V_N are shown to contribute more effectively to improving conductivity of the doped systems.

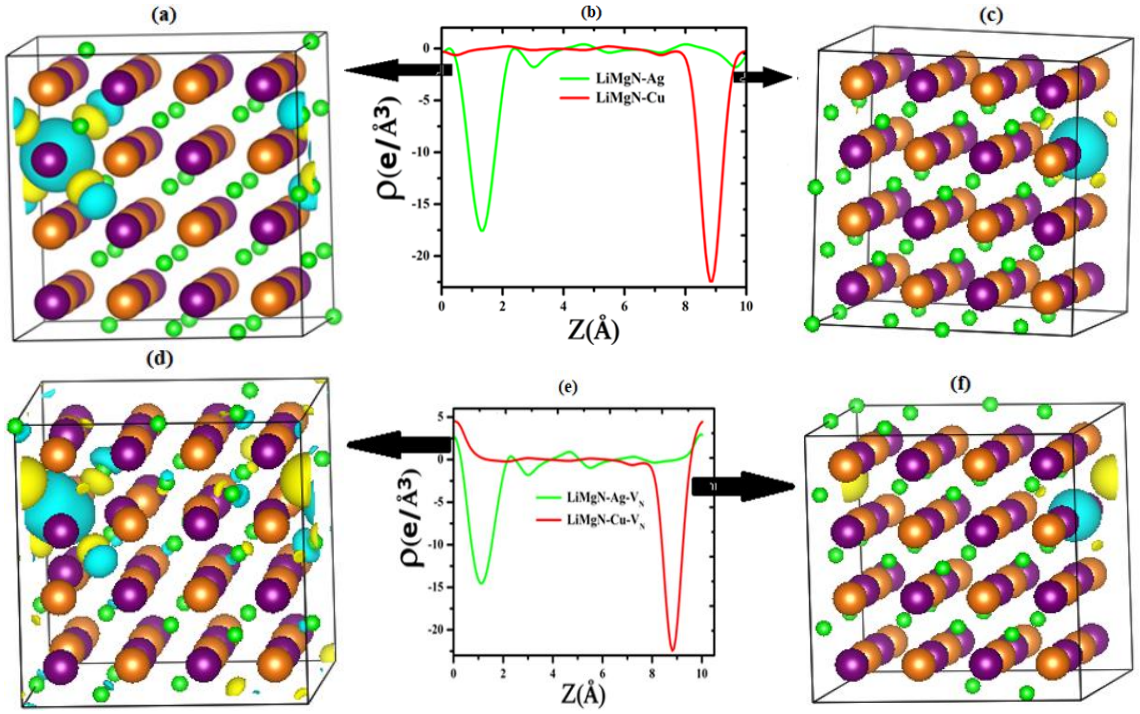

Fig. 4. Isosurface charge density plots of(a) LiMgN-Ag (c) LiMgN-Cu(d) LiMgN-Ag-V_N (f) LiMgN-Cu-V_N. Here purple, orange and green balls respectively represent Li, Mg and N atoms. Yellow and cyan colors represent charge accumulation and depletion. Integrated planer charged density plots of (b)Ag and Cu doped LiMgN (e) Ag and Cu doped+V_NLiMgN. Here green and red lines are representing Ag and Cu doped composites.

In Figure 5(a) represents isosurface charge density of LiMgN-Mn. Depletion of charge around dopant is observed in this case which is also confirmed from integrated planner charge density (green line) in Figure 5(b).Whereas, negative values of integrated charge density displayed by red line for LiMgN-Zn shows depletion of charge. This is also confirmed from isosurface charge density given in Figure 5(c). Magnetically doped LiMgN having V_N gives different behavior due to presence of nitrogen vacancy. Figure 5(d) represent isosurface charge density having depletion around dopant as well as accumulation is observed around V_N. This behavior is also confirmed from green line representing integrated planner charge density of LiMgN-Mn-V_N (Figure 5(e)). Here red line shows depletion around dopant in case of LiMgN-Zn-V_N. This depletion behavior is also confirmed from Figure 5(f). In Figure 2 DOS calculation also satisfied this behavior of Figure 5.Localization of conduction filaments(CFs) around dopant may be productive in overwhelming the random formation of CFs. Localization of CFs should contribution in incapacitating uniformity problems in electronic devices specifically RRAM devices [34]. By collecting and depleting additional charges, the nearest neighbor V_N and atom of the dopant are shown to contribute more effectively to improving conductivity of the doped systems. More conduction channels in case of LiMgN-Mn-V_N show that this composite might be more helpful for making more efficient RRAM.

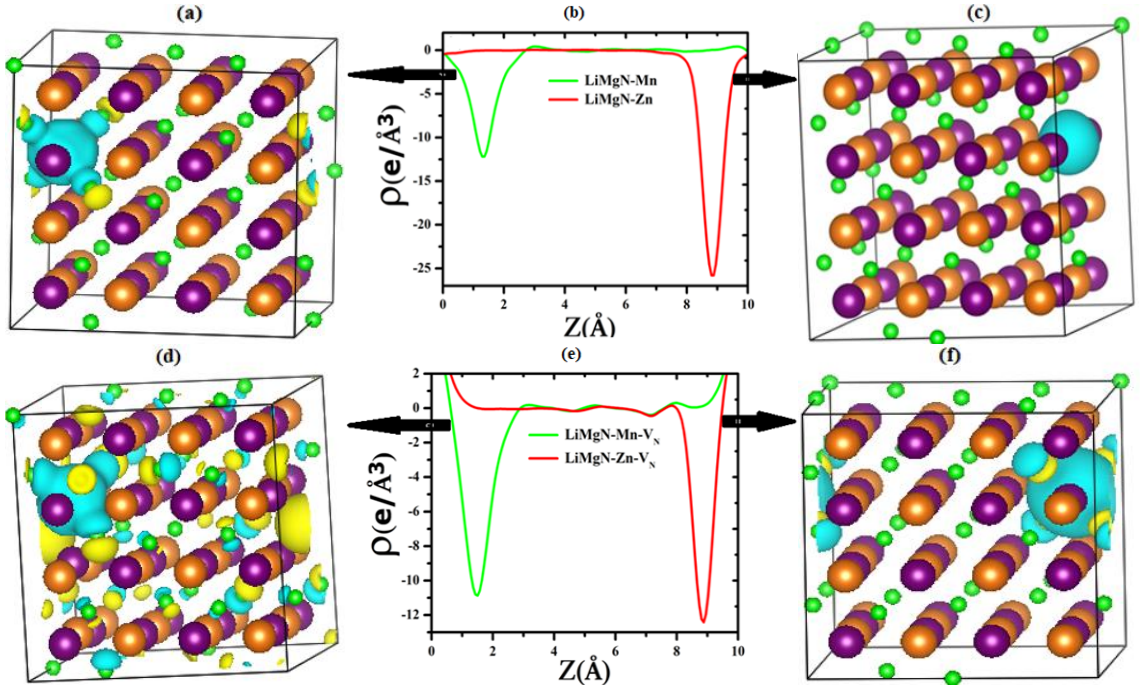

Fig. 5. Isosurface charge density plots of (a) LiMgN-Mn (c) LiMgN-Zn (d) LiMgN-Mn-V_N (f) LiMgN-Zn-V_N. Here purple, orange and green balls represent Li, Mg and N atoms, Yellow and cyan colors represent charge accumulation and depletion. Integrated planer charged density plots of (b) Mn and Zn doped LiMgN (e) Mn and Zn doped+V_NLiMgN. Here green and red lines are representing Ag and Cu doped composites.

5. Optical properties

With the help of optical properties interaction between incident photon energy and material can be observed. So, we examined complex dielectric function together with numerous other frequency dependent optical parameters, i.e., reflectivity (R(ω)), absorption coefficient (α(ω)), refractive index (n(ω)) and extinction coefficient (k(ω)), optical conductivity (σ(ω)) and energy loss function (L(ω)) of the studied composites to calculate its optoelectronic nature for countless applications specially in RRAM. Even though the dielectric function is a complex function, it is considered a significant parameter in the optical world. Dielectric function comprises of two parts [35] expressed as:

$$\varepsilon(\omega) = \varepsilon_1(\omega) + i\varepsilon_2(\omega) \tag{4}$$

Here, $\varepsilon_1(\omega)$ is real and $\varepsilon_2(\omega)$ is imaginary part of the dielectric function respectively. An electronic polarizability can be well clarified with the real part of the dielectric function. However, imaginary part of dielectric function calculates electronic absorption of incident light radiations over the material's surface.

The values calibrated for numerous optical parameters in the energy range 0-15 eV. Form Figure 6(a-f), static values of dielectric constant$\varepsilon_1(0)$for LiMgN, LiMgN-V_N, LiMgN-Ag, LiMgN-Ag-V_N, LiMgN-Cu, LiMgN-Cu-V_N, LiMgN-Mn, LiMgN-Mn-V_N, LiMgN-Zn and LiMgN-Zn-V_N at zero frequency calculated as 2.8, 3.3, 10.1, 3.2, 8.5, 5.7, 2.9, 3.4, 2.9 and 5.0 respectively. $\varepsilon_1(\omega)$ increase from critical value and approaches to maximum value of polarization i.e., LiMgN (4.30), LiMgN-V_N(4.5), LiMgN-Ag(4.1), LiMgN-Ag-V_N(5.0), LiMgN-Cu(3.7), LiMgN-Cu-V_N(4.0), LiMgN-Mn(4.3), LiMgN-Mn-V_N(4.2), LiMgN-Zn(4.2)and LiMgN-Zn-V_N(4.2) at 3.9 eV, 2.2 eV, 3.7 eV, 2.2 eV,3.3 eV, 2.5 eV,2.7 eV,1.6eV,3.7eV and 2.2 eV respectively.As the frequencies shift slightly, $\varepsilon_1(\omega)$ decreases abruptly and extend towards its negative values i.e., LiMgN (-1.7), LiMgN-V_N(-1.6), LiMgN-Ag (-1.4), LiMgN-Ag-V_N(-1.6), LiMgN-Cu (-1.2), LiMgN-Cu-V_N(-1.8), LiMgN-Mn (-1.5), LiMgN-Mn-V_N(-1.5), LiMgN-Zn (-

1.5) and LiMgN-Zn-V_N(-1.5) at 5.4 eV, 5.3 eV, 5.5 eV, 5.7 eV,5.2 eV, 5.3 eV,5.3 eV,5.8eV,5.3eV and 5.3 eV respectively. This exposes that interaction between free electrons of the materials and incident light (i.e., Plasmonic effect) is extreme at frequency that scatters the light falling on surface of material [36]. Then variations in the value of $\varepsilon_1(\omega)$ between 2- 6 eV happen due to diverse rates of transitions.

Imaginary part of dielectric function $\varepsilon_2(\omega)$ designates absorption of light in the material. From Figure 6(g-l) it is observed that at ω equals to zero, value of imaginary part of dielectric function becomes zero. After gaining threshold frequency, the value of $\varepsilon_2(\omega)$ increase drastically and gain maximum sharp peak at 4.4 eV, 4.5 eV, 4.7 eV, 4.6 eV, 4.4 eV, 4.5 eV, 4.4 eV, 4.4 eV, 4.7 eV, 4.5 eV for LiMgN, LiMgN-V_N, LiMgN-Ag, LiMgN-Ag-V_N, LiMgN-Cu, LiMgN-Cu-V_N, LiMgN-Mn, LiMgN-Mn-V_N, LiMgN-Zn and LiMgN-Zn-V_N respectively. This is a strong signal of absorption of incident light falling on the material surface wherever dispersion of light is nominal. The first microscopic dielectric function primarily defines the behavior of a material's linear response to an electromagnetic radiation field applied, revealing the material's absorptive nature.

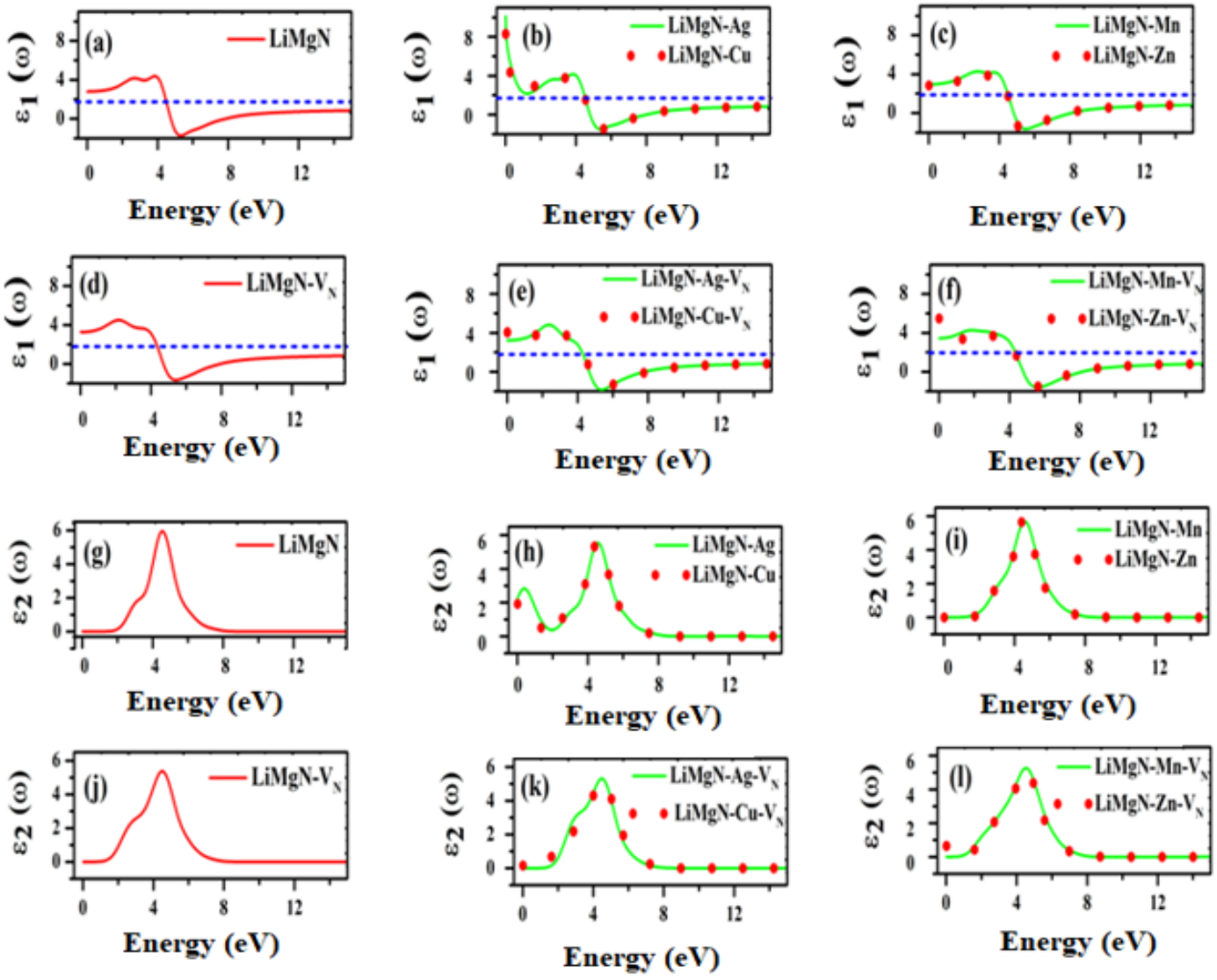

Fig. 6. Dielectric function verses energy plots (a-f) real part for$LiMg_{1-x}Y_xN$ (Y= Ag, Cu, Mn, and Zn) and (g-l) imaginary part for$LiMg_{1-x}Y_xN$-V_N (Y= Ag, Cu, Mn, and Zn).

By utilizing the following equations [37, 38] the values of refractive index $n(\omega)$as well as extinction coefficient k(ω) have been intended to approximate the material's tendency of transparency and absorption of incident photons for supplemental revelation:

$$n(\omega) = \frac{\left(\varepsilon_1 + (\varepsilon_1^2 + \varepsilon_2^2)^{\frac{1}{2}}\right)^{\frac{1}{2}}}{\sqrt{2}} \tag{5}$$

$$k(\omega) = \frac{\left(-\varepsilon_1 + (\varepsilon_1^2 + \varepsilon_2^2)^{\frac{1}{2}}\right)^{\frac{1}{2}}}{\sqrt{2}} \tag{6}$$

The static value of refractive index $n(0)$ calculated from Figure 7(a-f) are1.0,1.8,3.2,1.7,2.9,2.0,1.7,1.9,1.7 and 1.8 for LiMgN, LiMgN-V_N, LiMgN-Ag, LiMgN-Ag-V_N, LiMgN-Cu, LiMgN-Cu-V_N, LiMgN-Mn, LiMgN-Mn-V_N, LiMgN-Zn and LiMgN-Zn-V_N respectively. The peak values of refractive index for LiMgN (2.2), LiMgN-V_N(2.1), LiMgN-Ag (2.1), LiMgN-Ag-V_N(2.3), LiMgN-Cu (2.2), LiMgN-Cu-V_N(2.1), LiMgN-Mn (2.1), LiMgN-Mn-V_N(2.0), LiMgN-Zn (2.2) and LiMgN-Zn-V_N(2.1) appeared at 4.2 eV, 2.0 eV, 4.0 eV, 2.4 eV,4.0 eV, 3.3 eV,4.2 eV,2.6eV,4.0eV and 2.3 eV respectively. Consequently, for all cases, value of $n(\omega)$is decreasing steadily with increasing photonic energy ranging between 5.5-9.0 eV. At high energy upto 40eV, values of refractive index fluctuate owing to dissimilar rate of inner transition. The refractive index of a material is critical in production of photonic devices such as laser, quantum computers, optical fibers, photocatalysis, optical wave guides and light functioning diodes [39].

It is clear from Figure 7(g-l) that highest value of k(ω) for LiMgN (1.7), LiMgN-V_N(1.6), LiMgN-Ag (1.6), LiMgN-Ag-V_N(1.7), LiMgN-Cu (1.3), LiMgN-Cu-V_N(1.3), LiMgN-Mn (1.6), LiMgN-Mn-V_N(1.6), LiMgN-Zn (1.7) and LiMgN-Zn-V_N(1.5) at 4.9 eV, 4.8 eV, 5.1 eV, 4.9 eV,4.4 eV, 5.8 eV,5.0 eV,5.2eV,5.0eV and 5.3 eV respectively. Within ultraviolet region near incident photon energy range of 40 eV all composites to be behaved as a good absorber of the incident photons because small peak value of extinction appearance at this energy range.

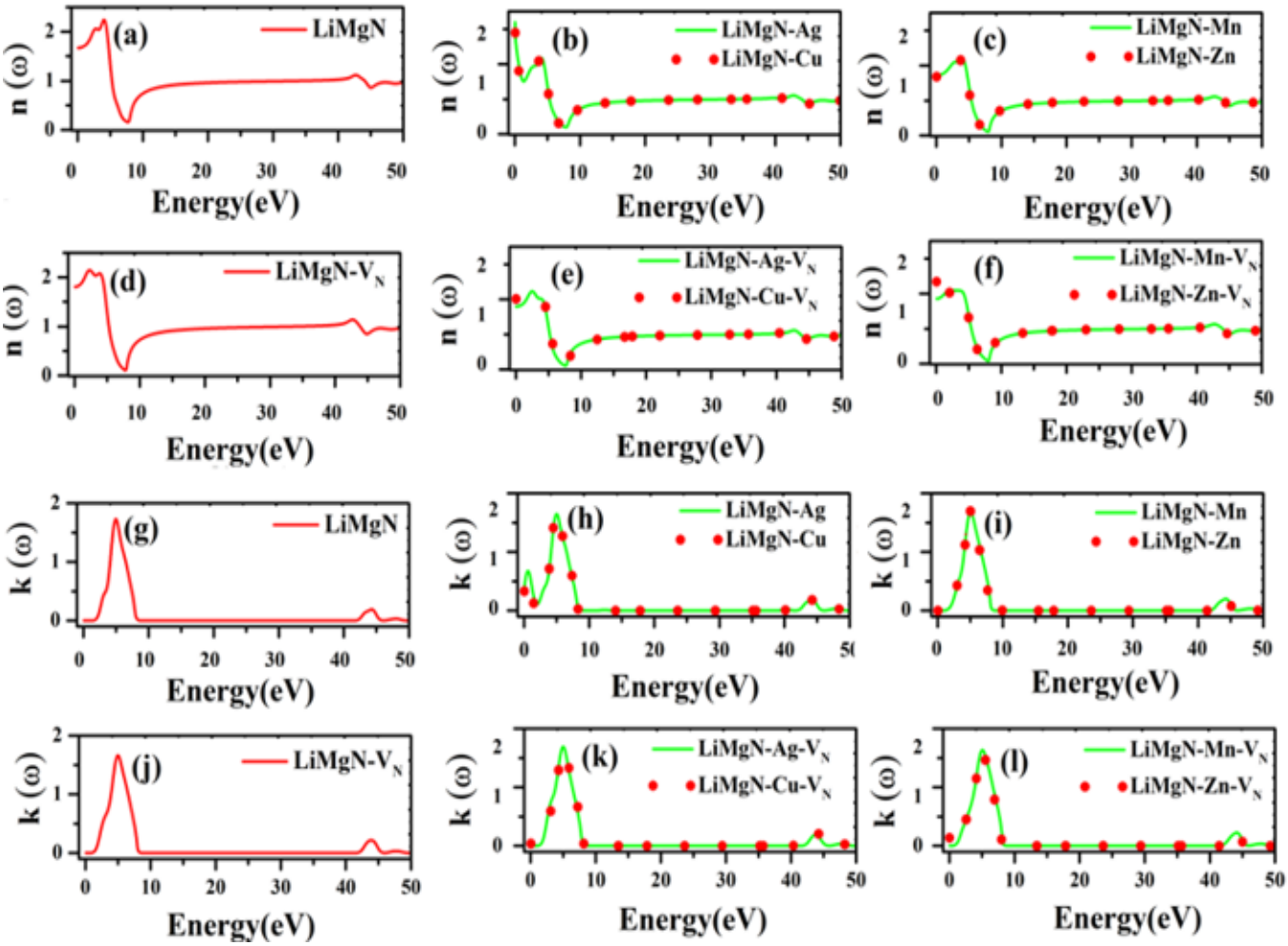

Fig. 7.(a-f) Real and (g-l) imaginary part of refractive index verses energy plots for $LiMg_{1-x}Y_xN$ *(Y= Ag, Cu, Mn, and Zn) and* $LiMg_{1-x}Y_xN$-V_N *(Y= Ag, Cu, Mn, and Zn).*

The reflectivity can be calculated by expressions [39]:

$$R(\omega) = \frac{(n-1)^2+k^2}{(n+1)^2+k^2} \quad (7)$$

Reflectivity represents the behavior of surfaces of studied compounds shown in Figure 8(a-f). The static value of reflectivity R(0) for LiMgN (0.06), LiMgN-V_N(0.08), LiMgN-Ag(0.08), LiMgN-Ag-V_N(0.09), LiMgN-Cu(0.06), LiMgN-Cu-V_N(0.08), LiMgN-Mn(0.07), LiMgN-Mn-V_N(0.10), LiMgN-Zn(0.07)and LiMgN-Zn-V_N(0.10).The momentous reflection happened in the locale of 7.7 eV photonic energy where absorptivity of material found to be low. Beyond this region it falls abruptly. Peak in the visible area is caused by electrons inner band transition.

The relation among $\alpha(\omega)$ is given as [36]:

$$\alpha(\omega) = \frac{2k\omega}{c} \quad (8)$$

It is clear from Figure 8(g-l) that value of $\alpha(\omega)$ remains zero for the photonic energy equal to the semiconductor's electronic energy band gap. Energy range emerging from origin showing zero absorption in the absence of light may be termed as zero photonic energy. Moreover, absorption of light in the material increases gradually with increasing the energy of incident photons. This increase is found to be of comparatively higher value in case of LiMgN-Mn-V_N. Absorption peak again appear at the energy of 45 eV for all cases. It is expected that LiMgN-Mn-

V_N composite would possibly well response and provide electromagnetic radiation absorption in the ultraviolet (UV) and visible ranges to realize material's behavior concerning the incident radiations. In all cases, it is observed that absorption peaks shift from visible range to UV region. Substantial absorption peaks over all doped systems indicate the presence of photo generated trapping centers exclusively at dopant defect sites. This guarantees that doped elements are used in optoelectronic devices, particularly optical memory systems. This absorbed energy might provide the necessary trigger for resistive devices to transition from HRS to LRS.

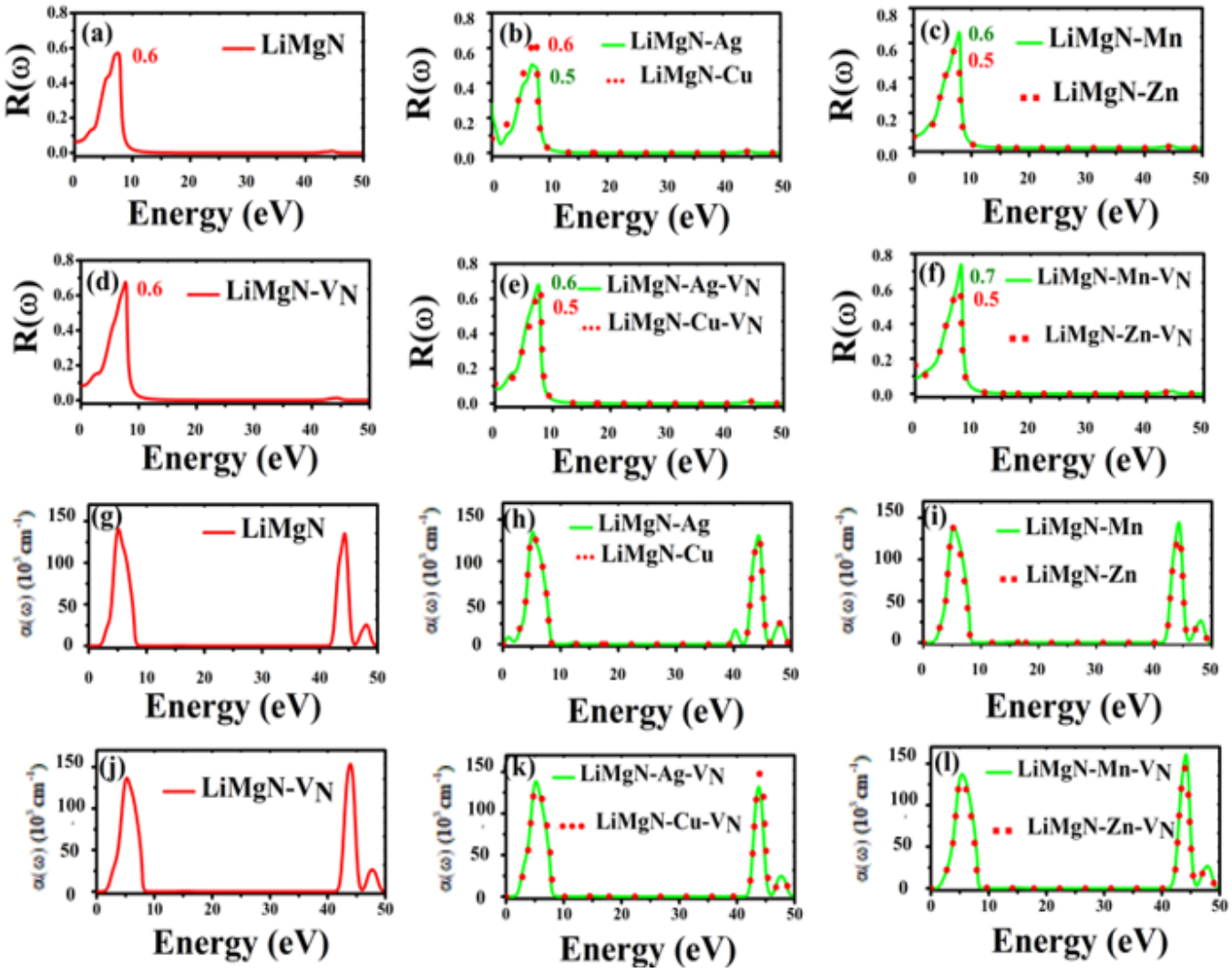

Fig. 8. (a-f) Reflectivity and (g-l) absorption verses energy plots for $LiMg_{1-x}Y_xN$ (Y= Ag, Cu, Mn, and Zn) and $LiMg_{1-x}Y_xN$-V_N (Y= Ag, Cu, Mn, and Zn) within the energy range 0-50 eV of incident electromagnetic radiations.

The optical conductivity can be calculated by expressions [40]:

$$\sigma(\omega) = \frac{\omega}{4\pi} Im\varepsilon(\omega) \tag{9}$$

The $\sigma(\omega)$ portrays that how bonds experience breakage as a result of incidence of photons with quantized energy on the surface of studied material. It is related with transition of electrons from valence to the conduction band as a result of photoelectric effect.

The optical conductivity defines conduction of light over materials depending upon inter and intra band transitions. It also talks about bond breaking when high energy electromagnetic

wave falls on materials surface. Optical conductivity behavior of the studied composites is displayed in Figure 9 (a-f). It follows almost analogous trend as that of absorptivity as shown in Figure 8. It has been observed that conductivity start increasing once photons of threshold frequency falls on materials surface. In all cases $\sigma(\omega)$ rise abruptly and reaches to maximum values. Improved optical conductivity for all cases precisely is lying in the energy range 8.0-42eV approximately for all composite due to different rate of inner transition. High value of optical conductivity for LiMgN-Mn-V_N exposes that this composite is good optical conductor in higher energy range directly above the threshold frequency. Relative results display distinctive conductivity in case of LiMgN-Mn-V_N thus, it is considered appropriate material for potential tenders in photovoltaic's and additional optoelectronic devices.

The loss function calculation is used to approximate loss of photonic energy as a consequence of high-speed electronic transition [37] and is associated to the dielectric function as [41]:

$$L(\omega) = \frac{\varepsilon_2(\omega)}{\varepsilon_1^2(\omega)+\varepsilon_{2(\omega)}^2} \tag{10}$$

The photoelectrons-transient electrons interaction reasons the loss of energy termed Plasmonic losses.

The photoelectrons-transient electrons interaction reasons the loss of energy termed as plasmonic losses. The energy loss radically increases beyond the energy of 6-9eV for all cases. Plasmon peaks (max energy loss for all composite exposed in Figure 9 (g-l), lie in the high energy region. Because the frequency of the incoming photons is greater than the plasma frequency, the material becomes transparent beyond this energy range. Highest transition of electrons is observed for LiMgN-Mn-V_N. The graph also shows that when considerable absorption of incoming photons in the material surface has been detected, energy loss is low.

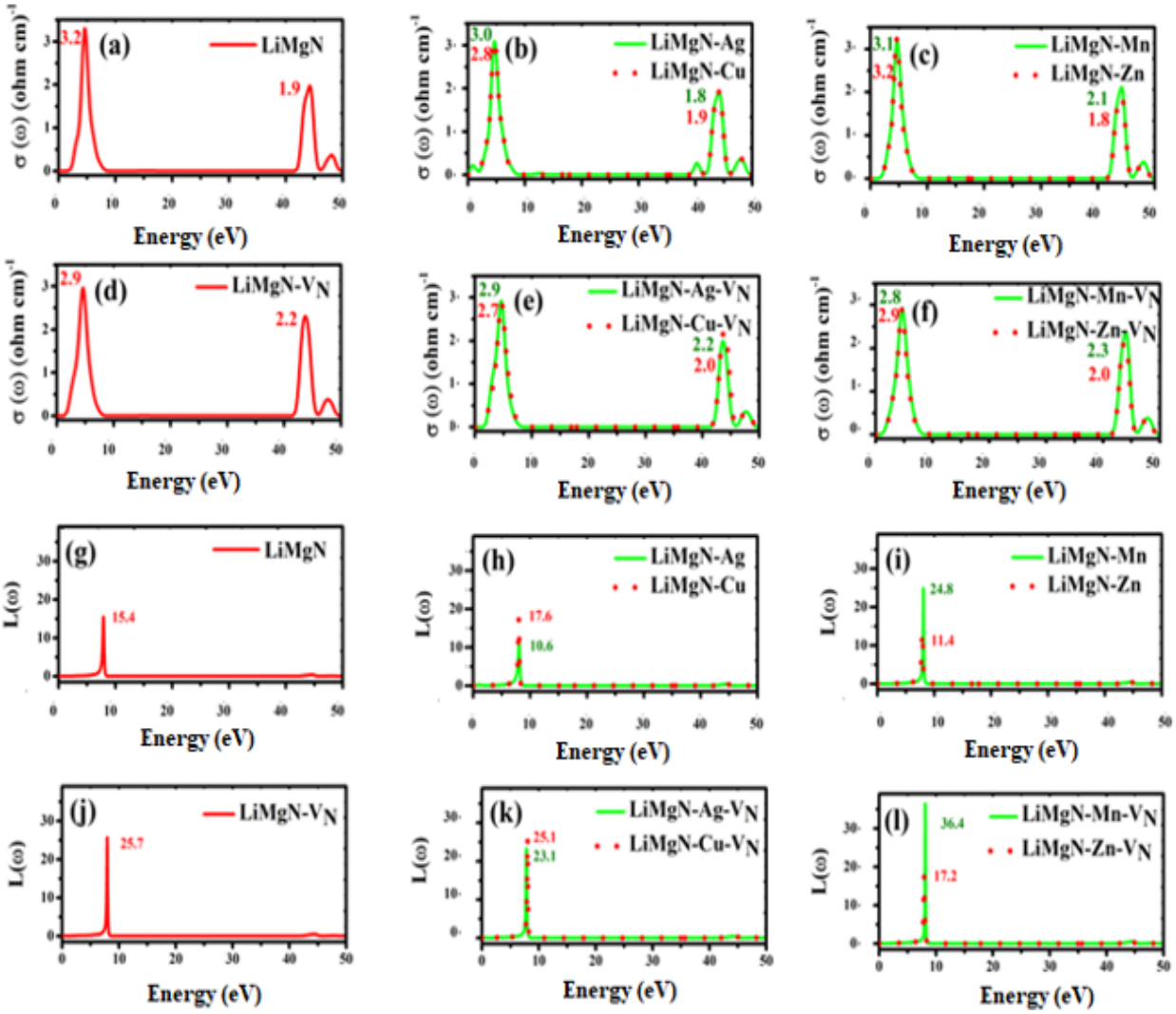

Fig. 9. (a-f) Conductivity and (g-l) loss function verses energy Plots for $LiMg_{1-x}Y_xN$ (Y= Ag, Cu, Mn, and Zn) and $LiMg_{1-x}Y_xN$-V_N (X= Ag, Cu, Mn, and Zn) within the energy range 0-50 eV of incident electromagnetic radiations.

6. Conclusion

The formation energy, electronic and optical characteristics of $LiMg_{1-x}Y_xN$ (Y = Ag, Cu, Mn, Zn) has been calculated using DFT approach for application of RRAM devices. The DOS plots revealed increased conductivity of the doped systems. By receiving and releasing electrons, the V_N near dopant played a key part in enhancing conductivity for LiMgN-Mn-V_N.CFs formed around dopants can inhibit the random production of CFs in electrode materials. The estimated electronics characteristics, isosurface charge density, and integrated charge density reveal that LiMgN-Mn-V_N is more stable and conductive than other doped systems in terms of stability and conductivity. The development of conductive filaments (conductive route) might play significant role in fulfilling the RS events as a result of this charge redistribution. The optical characteristics of the doped systems revealed that conductivity maxima have been localized within visible and low-energy ultraviolet incident radiations. LiMgN-Mn-V_N was shown to be the best composite for RRAM applications and in optoelectronic applications.

References

[1] Y. S. Chen, B. Chen, B. Gao, L. F. Liu, X. Y. Liu, and J. F. Kang, Applied Physics. 113, 164507 (2013); https://doi.org/10.1063/1.4803076

[2] F. Hussain, M. Imran, R.M.A. Khalil, M.A. Sattar, N.A. Niaz, A.M. Rana, M. Ismail, E.A. Khera, U. Rasheed, F. Mumtaz, T. Javed, S. Kim, Vacuum. 168(10),108842 (2019); https://doi.org/10.1016/j.vacuum.2019.108842

[3] L. Sun, X. Hao, Q. Meng, L. Wang, F. Liu, and M. Zhou, Adv. Electron. Mater. 1900271(2019); https://doi.org/10.1002/aelm.201900271

[4] Hu Q, Park MR, Abbas H, Kang TS, Yoon TS, Kang C J, Microelectron. Eng. 190,7-10 (2018); https://doi.org/10.1016/j.mee.2018.01.005

[5] N. S. Masuri, R. Ahmed, A. Shaari, B.Ul Haq, M. Mohamad, A. Hussain, M. N. Muhamad, Journal Teknologi. 78:3,111-116 (2016); https://doi.org/10.11113/jt.v78.7475

[6] K. Kuriyama, T. Kato, and K. Kawada, Phys. Rev. B 49, 11452 (1994); https://doi.org/10.1103/PhysRevB.49.11452

[7] F. Kalarasse and B. Bennecer, J. Phys. Chem. Sol. 67, 846 (2006); https://doi.org/10.1016/j.jpcs.2005.12.005

[8] W. Bockelmann and H.-U. Schuster, Z. Anorg. Allg. Chem. 410, 241 (1974); https://doi.org/10.1002/zaac.19744100304

[9] K. Kuriyama, R. Taguchi, K. Kushida, and K. Ushiyama, J. Cryst. Growth. 198, 802 (1999); https://doi.org/10.1016/S0022-0248(98)00984-1

[10] J. J. Martin, Phys. Chem. Sol. 33, 1139 (1972); https://doi.org/10.1016/S0022-3697(72)80273-7

[11] K. Kuriyama, K. Nagasawa, and K. Kushida, J. Crys. Growth. 237-239, 2019 (2002); https://doi.org/10.1016/S0022-0248(01)02249-7

[12] J. Barth, G. H. Fecher, M. Schwind, A. Beleanu, C. Felser, A. Shkabka, H. Wedenkaff, J. Hanss, A. Reller, and M. K€ohne, J. Electron. Mater. 39(9), 1856 (2010); https://doi.org/10.1007/s11664-010-1076-9

[13] H.-P. Li, Z.-F. Hou, M.-C. Huang, Z.-Z. Zhu, Chin. Phys. Lett. 20, 114 (2003); https://doi.org/10.1088/0256-307X/20/1/334

[14] L.H. Yu, K.L. Yao, Z.L. Liu, Physica B. 353, 278 (2004); https://doi.org/10.1016/j.physb.2004.10.008

[15] L.H. Yu, K.L. Yao, Z.L. Liu, Solid State Commun. 135, 124 (2005); https://doi.org/10.1016/j.ssc.2005.03.041

[16] H.C. Kandpal, C. Felser, R. Seshardri, J. Phys. D Appl. Phys. 39, 776 (2006); https://doi.org/10.1088/0022-3727/39/5/S02

[17] A. Walsh, S.-H. Wei, Phys. Rev. B. 76, 195208 (2007); https://doi.org/10.1103/PhysRevB.76.195208

[18] F. Kalarasse, B. Bennecer, A. Mellouki, J. Phys. Condense. Matter.18, 7237; https://doi.org/10.1088/0953-8984/18/31/018

[19] M. Arif, G. Murtaza, R. Ali, R. Khenata, Y. Takagiwa, M. Muzammil and S. B. Omran, Indian J Phys. (2015).

[20] Y. Sun, C. Song, S. Yin, L. Qiao, Q. Wan, J. Liu, R. Wang, F. Zeng, F. Pan, ACS Appl Mater Interfaces. 12(26), 29481-29486 (2020).

[21] Y. ZB, J.M. Liu, Ann Phys. 358, 206-224 (2015); https://doi.org/10.1016/j.aop.2015.03.028

[22] JP Perdew, K Burke, M Ernzerhof, Phys. Rev. Lett. 77,3865 (1997); https://doi.org/10.1103/PhysRevLett.77.3865

[23] Blochl PE. Projector Augmented-Wave Method. Phys. Rev. B. 47, 558 (1993).

[24] G Kress, D Joubert, Phys. Rev. B. 59,1758 (1999); https://doi.org/10.1103/PhysRevB.59.1758

[25] A V. Krukau, A Oleg, OA Vydrov, A F. Izmaylov, and G E. Scuseriaa, J. Chem. Phys. 125, 224106 (2006); https://doi.org/10.1063/1.2404663

[26] HJ Monkhorst, JD Pack, Phys. Rev. B. 13, 5188 (1976); https://doi.org/10.1103/PhysRevB.13.5188
[27] HJ Monkhorst, JD Pack, Phys. Rev. B. 16,1748 (1977); https://doi.org/10.1103/PhysRevB.16.1748
[28] S. Alireza, V.M. Ali, B. Mahsa, M. Anis Physica B. 430, 20-26 (2013).
[29] F. Hussain, M. Imran, U. Rasheed, R.M.A. Khalil, A.M. Rana, K. Farhana, A.J. Muhammad, S.S. Hayat, J. Electron. Mater. 32, 2343-2349 (2019); https://doi.org/10.1007/s11664-019-07064-2
[30] U. Resheed, T. Alsuwian, M. Imran, H. Algadi, E.A. Khera, R.M.A. Khalil, C. Mahata, F. Hussain Int J Energy Res. 45(7), 10882-10894 (2021); https://doi.org/10.1002/er.6572
[31] F. Yang, L. Yang, A. Changzhi, P. Xie, S. Lin, C.Z. Wang, X. Lu, Nanomaterials. 8(7), 455 (2018); https://doi.org/10.3390/nano8070455
[32] Y.T. Azar, M. Payami, Appl. Surf. Sci. 412, 335-341(2017); https://doi.org/10.1016/j.apsusc.2017.03.147
[33] B. Chilukuri, U. Mazur, K.W. Hipps, Phys. Chem. Chem. Phys. 16(27), 14096 (2014); https://doi.org/10.1039/C4CP01762E
[34] T. Tan, A. Cao, G. Zha, Superlattice Microst. 121, 38-44 (2018); https://doi.org/10.1016/j.spmi.2018.07.022
[35] M. H. Samat, A.M.M Ali, M. F. M. Taib, O. H. Hassan, M. Z. A. Yahya, Phys.6,891-896 (2016); https://doi.org/10.1016/j.rinp.2016.11.006
[36] B. Sabir, G. Murtaza, R.M. Arif Khalil, Q. Mahmood, J. Mol. Graph. Model. 86, 19-26 (2019); https://doi.org/10.1016/j.jmgm.2018.09.011
[37] M. Fox, Classical propagation, OUP Inc. New York. 25-48 (2001).
[38] M. Dressel, G. Grüner, CUP. UK. 1269-1270 (2002); https://doi.org/10.1119/1.1516200
[39] E.A. Khera, H. Ullah, M. Imran, N.A. Niaz, F. Hussain, R.M.A. Khalil, U. Rasheed, M.A. Sattar, F. Iqbal, C. Mahta, A.M. Rana, S. Kim, Optik. 212, 164677 (2020); https://doi.org/10.1016/j.ijleo.2020.164677
[40] A. H. Reshak, Z. Charifi, H. Baaziz, J. Solid State Chem.183(6),1290-1296 (2010); https://doi.org/10.1016/j.jssc.2010.03.029
[41] S. Saha, T. P. Sinha, A. Mookerjee, Phy.Rev.B.62 (13), 8828 (2000); https://doi.org/10.1103/PhysRevB.62.8828